Rapid Cycling and Exceptional Yield in a Metal-Organic Framework Water Harvester

Nikita Hanikel,[†,‡,§,||,∇] Mathieu S. Prévot,[†,‡,§,||,∇] Farhad Fathieh,[†,‡,§,||] Eugene A. Kapustin,[†,‡,§,||] Hao Lyu,[†,‡,§,||] Haoze Wang,[†,‡,§,||] Nicolas J. Diercks,[†,‡,§,||] T. Grant Glover,[⊥] and Omar M. Yaghi*[†,‡,§,||,#]

[†]Department of Chemistry, University of California—Berkeley, Berkeley, California 94720, United States

[‡]Materials Sciences Division, Lawrence Berkeley National Laboratory, Berkeley, California 94720, United States

[§]Kavli Energy NanoSciences Institute, Berkeley, California 94720, United States

[||]Berkeley Global Science Institute, Berkeley, California 94720, United States

[⊥]Department of Chemical and Biomolecular Engineering, University of South Alabama, Mobile, Alabama 36688, United States

[#]UC Berkeley−KACST Joint Center of Excellence for Nanomaterials for Clean Energy Applications, King Abdulaziz City for Science and Technology, Riyadh 11442, Saudi Arabia

Ⓢ Supporting Information

ABSTRACT: Sorbent-assisted water harvesting from air represents an attractive way to address water scarcity in arid climates. Hitherto, sorbents developed for this technology have exclusively been designed to perform one water harvesting cycle (WHC) per day, but the productivities attained with this approach cannot reasonably meet the rising demand for drinking water. This work shows that a microporous aluminum-based metal-organic framework, MOF-303, can perform an adsorption–desorption cycle within minutes under a mild temperature swing, which opens the way for high-productivity water harvesting through rapid, continuous WHCs. Additionally, the favorable dynamic water sorption properties of MOF-303 allow it to outperform other commercial sorbents displaying excellent steady-state characteristics under similar experimental conditions. Finally, these findings are implemented in a new water harvester capable of generating 1.3 L kg_{MOF}^{-1} day^{-1} in an indoor arid environment (32% relative humidity, 27 °C) and 0.7 L kg_{MOF}^{-1} day^{-1} in the Mojave Desert (in conditions as extreme as 10% RH, 27 °C), representing an improvement by 1 order of magnitude over previously reported devices. This study demonstrates that creating sorbents capable of rapid water sorption dynamics, rather than merely focusing on high water capacities, is crucial to reach water production on a scale matching human consumption.
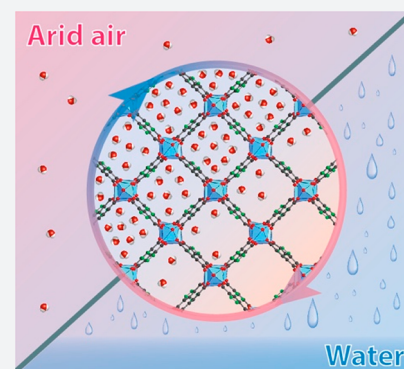
■ INTRODUCTION

Access to water is crucial for improving health, standards of living, and productivity worldwide.[1,2] However, it is expected that, by the year 2050, 50% of the world population will experience water stress due to contamination of surface water and depletion of underground reservoirs.[2–6] In this context, techniques to produce clean water from alternative sources are desirable, especially in arid regions, where it is most needed.[6,7] Water harvesting from air has the potential to provide potable water with minimal generation of waste and can be implemented off the grid at any location, due to the ubiquitous presence of vapor in the atmosphere. While direct extraction is easily achieved in humid climates by fog harvesting or through condensation by cooling air below its dew point, it is unfeasible and energy-intensive in arid environments.[8,9] One way to circumvent this limitation is to engineer an adsorbent-assisted water harvesting cycle (WHC), where water vapor from an arid air feed is first concentrated in a sorbent and subsequently released to a condenser. Previously, we applied this principle by using metal-organic frameworks (MOFs) as sorbents in water harvesting units.[10–12] These devices performed only one WHC per day (adsorption at night and desorption during the daytime) and therefore delivered small amounts of water, limited by the sorbent's capacity. To realize the vast potential of water harvesting from desert air, a system capable of multiple cycles per day must be designed. Accordingly, fast kinetics of water uptake and release in a sorbent material becomes of paramount importance to yield significantly larger amounts of water. However, work in this field has largely focused on the equilibrium water sorption capacity of a material or on tuning the sorption isotherm shape,[13–18] rather than the kinetics of the WHC, which is an aspect we address here.
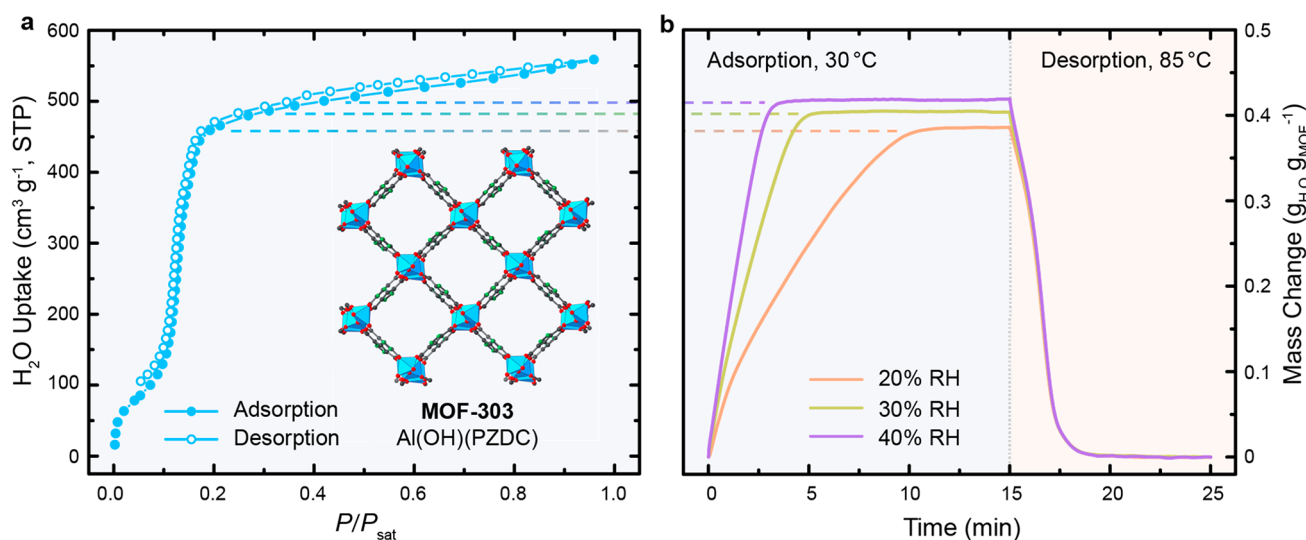
Figure 1. Water sorption properties of MOF-303. (a) Water sorption isotherm at 30 °C. (Inset: structure of MOF-303 [Al(OH)(PZDC), PZDC = 1H-pyrazole-3,5-dicarboxylate].[12] Hydrogen atoms are omitted for clarity. Color code: Al, blue; C, gray; O, red; N, green.) (b) Dynamic vapor sorption properties of a thin MOF layer: adsorption at 30 °C and 20−40% relative humidity (RH) and subsequent desorption at 85 °C and 0% RH.

In this report, we studied the water sorption kinetics of several microporous materials, and we found that an aluminum-based MOF, MOF-303 [Al(OH)(PZDC), PZDC = 1H-pyrazole-3,5-dicarboxylate], outperforms commercial sorbents suitable for water uptake in arid environments (zeolite 13X, SAPO-34, Basolite A520 [Al-fumarate]) and emerges as the most favorable candidate for efficient water harvesting through rapid cycling. We used these findings to engineer a new water harvester, capable of continuous operation, conducting multiple adsorbent-assisted WHCs per day that can be powered by solar electricity. When this system is equipped with MOF-303, it generates 1.3 L kg_{MOF}^{-1} day^{-1} in an indoor arid environment (27 °C, 32% relative humidity, RH). Remarkably, this harvester can operate for days in the hyperarid environment of the Mojave Desert, where it produces water with 1 order of magnitude increase in productivity (0.7 L kg_{MOF}^{-1} day^{-1}) compared to the previous study in an outdoor desertic environment.[12] Our work firmly establishes how atmospheric water can be harvested and delivered to regions facing severe water stress.

RESULTS AND DISCUSSION

Microporous MOFs have been identified as promising materials for atmospheric water harvesting due to their high water uptake, and rich chemical variability and tunability stemming from the principles of reticular chemistry.[19−22] An excellent example of such a material is MOF-303. The PZDC linker renders this material hydrophilic, with a water uptake of 39 wt% at 20% RH and an inflection point at ~12% RH, making it a viable water adsorbent in a desert environment. This MOF exhibits minimal to no hysteresis in its water sorption behavior (Figure 1a) and an isosteric heat of adsorption of ~52 kJ mol^{-1} (Figure S25), allowing for high working capacity and facile regeneration. Additionally, construction from rod-like aluminum-based secondary building units (SBUs) makes this material hydrolytically stable, which is reflected by the fact that there is no measurable decrease in capacity after 150 adsorption−desorption cycles.[12] Initial dynamic adsorption tests conducted on a thin layer of this MOF with the help of a thermogravimetric analyzer (TGA)

under constant humidified air flow (see the Methods section for details) revealed full saturation at 20% RH after ~10 min (5 and 3 min at 30 and 40% RH, respectively; Figure 1b, left) and subsequent complete regeneration within a few minutes through mild heating (85 °C; Figure 1b, right).

To put these results in perspective with the dynamic sorption performance of other microporous materials, we conducted a comparative study aiming at determining which material had the best properties to perform fast WHCs. We focused on comparing MOF-303 to commercial sorbents; however, other sorbents might also be interesting candidates for such a benchmark testing.[13,20,23−27] The selected materials were MOF-303, Al-fumarate [Al(OH)(fumarate)], Basolite A520, BASF SE],[28] and the zeolites SAPO-34 and zeolite 13X, all hydrophilic materials viable for water uptake under arid conditions, as made evident by their respective water sorption isotherm (Figure 2). Additionally, MOF-303, Al-
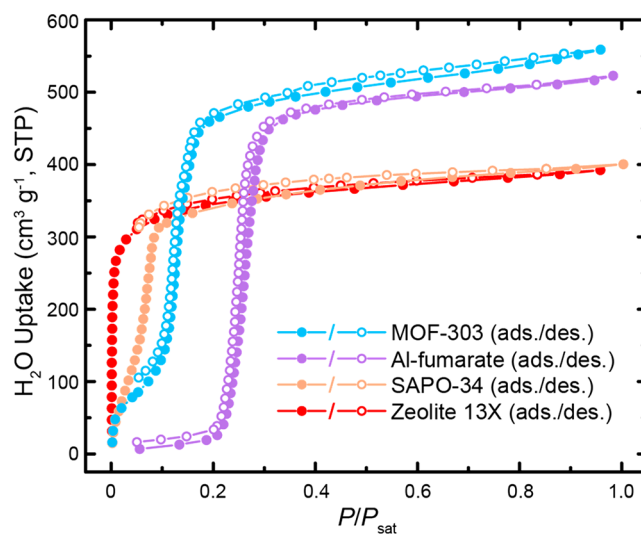

Figure 2. Water sorption isotherms at 30 °C of the tested materials. P, partial water vapor pressure; P_{sat}, saturation water vapor pressure at 30 °C. STP: standard temperature and pressure.
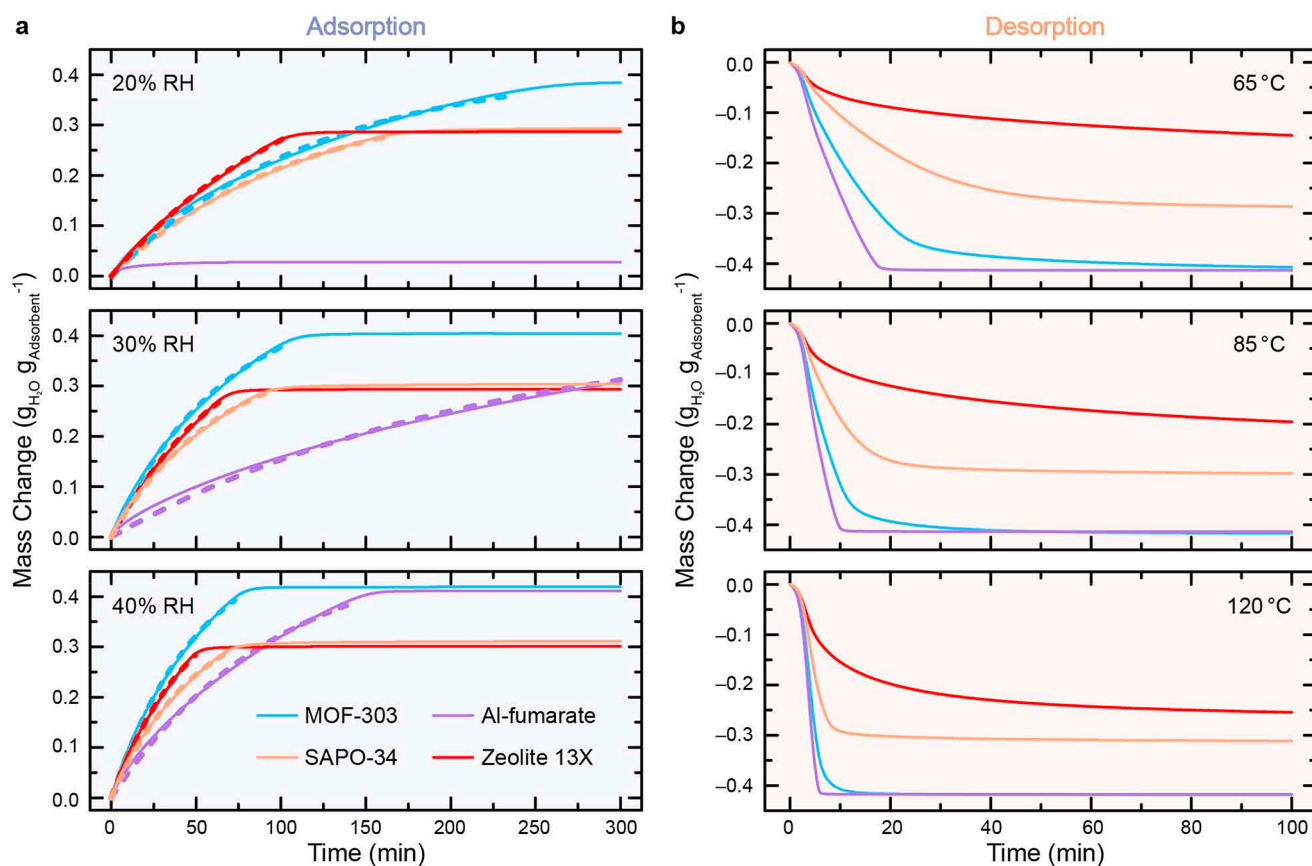
Figure 3. Experimental data is represented by solid lines. The line color indicates the type of sorbent, as specified in the inset. (a) Water adsorption at 30 °C and 20−40% relative humidity (RH). Prior to adsorption, the sorbent materials were fully dehydrated. The initial 95% filling is approximated with a monoexponential fit (dashed lines in the respective color). The curve for Al-fumarate at 20% RH was not fitted due to insufficient water uptake at this RH. (b) Water desorption at 65, 85, and 120 °C, and 0% RH. Prior to desorption, the sorbent materials were saturated at 30 °C and 40% RH.

fumarate, and SAPO-34 exhibited moderate heats of adsorption (50−54 kJ mol^{-1}, see Section S3.2 for details), allowing for thermodynamically facile regeneration of these sorbents. For the comparison of the dynamic water sorption properties, we chose to process the sorbent powder in a thin packed bed geometry. This processing method had the advantages of being quick and highly reproducible. Also, using it allowed us to limit the number of parameters to optimize. Indeed, an accurate comparison of the dynamic water sorption properties between different sorbents can be challenging, because, in addition to the intrinsic material characteristics, geometric and morphological factors of the sorbent can contribute to deviations in the overall kinetic performance. The thickness and packing porosity of the sorbent bed,[10] as well as the grain size,[29] are all important parameters to control in this context. Consequently, in this study, the materials were all processed in layers with a constant height of 3 mm and a packing porosity of 0.7—avoiding the Knudsen regime for the intercrystallite diffusion while achieving a high volumetric water capture capacity, as identified in our previous work (see the Methods section for details about the experimental setup).[10] The sorbent density, necessary for accurate adaptation of the targeted packing porosity, was determined by using argon sorption measurements and helium gas pycnometry (see Sections S2.3 and S2.4 for details). Furthermore, the grain size of each MOF matched the zeolite particle size (2−5 μm diameter, Section S2.2).

The dynamics of water vapor sorption were assessed under a range of conditions for the four materials, and reproducibility of the results was verified by duplicate measurements (Section S4.3). The sorbents were dehydrated prior to each adsorption measurement, and the water uptake was monitored at 30 °C and 20−40% RH (Figure 3a, see the Methods section for details). The water uptake over time exhibited an apparent monoexponential behavior that was fitted accordingly (with R^2 > 99% for all fits, see Figure 3a and Section S4.4). We found that the initial adsorption rate, R_0, accurately, although qualitatively, reflects the gravimetric water uptake behavior at any given time (Figure 3a), which can be appreciated when considering the apparent monoexponential nature of the adsorption curves. We use the corresponding normalized value $R_{0,norm}$ (normalized to 1.0 for MOF-303 at 20% RH) hereafter to discuss and compare the kinetic adsorption properties of the candidate materials. The desorption behavior was not approximated by a function due to interference of the fast, but not instantaneous, TGA oven temperature increase with the simultaneous, rapid desorption process exhibited by some materials (e.g., Al-fumarate). Nevertheless, clear desorption kinetic trends were also observed (Figure 3b).

As expected, the water adsorption process becomes faster with increasing RH for all tested materials, but different trends in the relative performances of the different sorbents were observed at different humidities (Table 1). Indeed, at 20% RH, zeolite 13X outperforms the other materials tested in this study

Table 1. Quantification of the Dynamic Water Adsorption Behavior at Different Relative Humidities[a]

adsorbent	RH (at 30 °C, %)	$R_{0,norm}$
MOF-303	20	1.0
	30	2.1
	40	2.9
Al-fumarate	30	0.6
	40	1.5
SAPO-34	20	0.9
	30	1.7
	40	2.2
zeolite 13X	20	1.2
	30	1.8
	40	2.6

[a]$R_{0,norm}$: normalized initial rate of adsorption (normalized to 1.0 for MOF-303 at 20% relative humidity, RH).

($R_{0,norm}$ = 1.2). While this behavior could be attributed to the strong hydrophilicity of the material, reflected in its Type I water sorption isotherm (Figure 2), we also note that MOF-303 exhibits more favorable adsorption kinetics than SAPO-34 (1.0 versus 0.9, respectively), despite the inflection point of the latter lying at lower relative pressures. The uptake of Al-fumarate at this RH is negligible and thus was not considered in the quantitative comparison. At higher RH (30% and 40%), the adsorption kinetics of MOF-303 becomes most favorable (2.1 and 2.9), followed by zeolite 13X (1.8 and 2.6) and SAPO-34 (1.7 and 2.2). Al-fumarate exhibits very slow adsorption kinetics at 30% RH (0.6)—close to the inflection

point in its water sorption isotherm (Figure 2). Under the given experimental setup, it equilibrates only after ∼10 h (Figure S33). Strikingly, even at 40% RH, despite its water uptake, pore diameter, and pore volume being comparable to MOF-303 (Figure 2 and Table S1), Al-fumarate exhibits much less favorable dynamic vapor adsorption properties (1.5) compared to MOF-303 and the zeolites (Figure 3a). This behavior could stem from its less hydrophilic nature, reflected in its inflection point lying at a relatively high partial vapor pressure (Figure 2). Importantly, these findings illustrate that the total water uptake of a given material at a given humidity does not necessarily predetermine its adsorption dynamics. Therefore, a rigorous investigation of the dynamic vapor sorption properties of recently reported MOFs displaying impressive water uptakes under arid and semiarid conditions would be very instructive to evaluate their potential performance in a device relying on fast WHC.[13,15,17,18,20]

Prior to desorption, all samples were equilibrated at 30 °C and 40% RH to ensure comparability between the measurements, and the desorption process was then monitored at 0% RH and temperatures ranging from 65 to 120 °C. As anticipated, water desorbed faster at higher temperatures. At 65 °C, complete dehydration required only 20 min for Al-fumarate (Figure 3b) and several hours for MOF-303 (Figure S32), while the zeolites remained partially saturated within the time frame of the measurement (Figures S36 and S38). MOF-303 becomes more competitive at 85 °C with a complete desorption time of ∼1 h, which can be further shortened at higher temperatures (Figure 3b). In contrast, complete
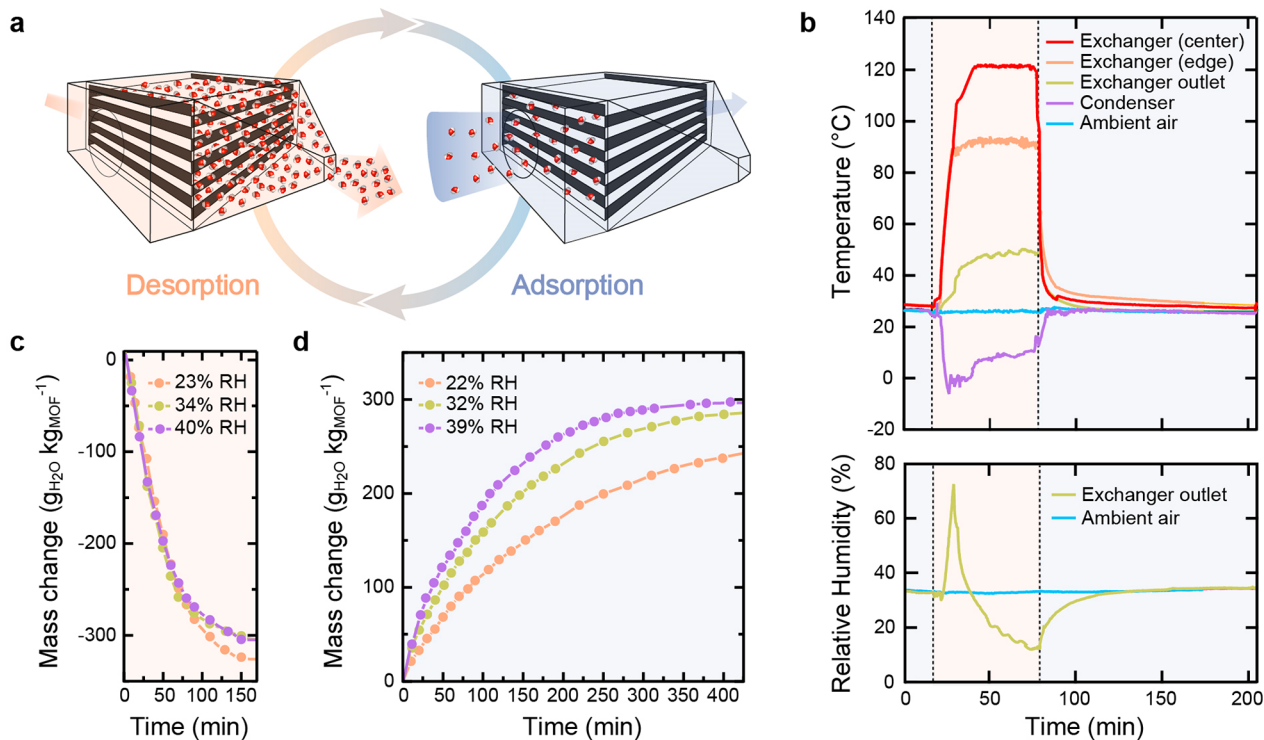

Figure 4. Water harvesting cycle (WHC) as operated by the atmospheric water harvester. (a) Illustration of the WHC. During the desorption step, the MOF bed is heated to release water vapor, which is immediately transferred to the condenser under convective air flow. During the adsorption step, ambient air is propelled, through forced convection across the exchanger, to facilitate mass transfer to the MOF. (b) Evolution of temperature and relative humidity (RH) during a typical WHC, as measured by sensors at different locations in the harvester. Measured desorption (c) and adsorption (d) kinetics, in terms of mass of water per mass of sorbent against time, measured for MOF-303 under different ambient RH. The ambient temperature was measured to be 25 ± 2 °C for all experiments.

dehydration of SAPO-34 can only be achieved by heating to temperatures above 100 °C (Figure S36), and zeolite 13X, the material showing the most attractive adsorption performance under hyperarid conditions, could not be fully desorbed within 10 h, even at 120 °C (Figure S38). This signals an important limitation of the working capacity of zeolite 13X under mild desorption temperatures. For instance, a decrease of ∼30% in the working capacity is expected if the zeolite is desorbed at 85 °C for 2 h (Figure 3). Additionally, the next adsorption cycle would necessarily start with a partially saturated material, which, due to the exponential nature of the process, would result in a consequent slowdown in its cycling dynamics.

It is important to note that the diffusion rate of water molecules in these microporous materials could be different at different locations on the water sorption isotherm (e.g., at the inflection point versus in the saturation region), making a fully quantitative rationalization of the observed behavior challenging.[21,30,31] Moreover, heat transfer, mass transfer, and diffusion processes likely affect the overall water uptake dynamics that were measured, and some of these phenomena may become more prevalent when the sorption takes place in a packed column or another configuration different than a thin-layer geometry (as exemplified by the comparison between Figures 1b and 3).[32] More advanced techniques, such as IR microimaging, frequency response techniques, or zero length column methods, would be required for the determination of the diffusion constants and mechanism,[30,32−35] which is an intriguing objective for future research. Nevertheless, the experimental results presented here provided an appropriate simulation of the expected dynamic adsorption and desorption behavior of each sorbent when cycled rapidly under arid conditions, allowing us to predict which material was the best candidate for the targeted application, namely, MOF-303. Indeed, it exhibited a good performance at 20% RH, only outperformed by the highly hygroscopic zeolite 13X, and it displayed the fastest uptakes at 30% and 40% RH. Further, a 3 mm packed bed of MOF-303 was completely dehydrated within minutes of mild heating (85−100 °C).

We therefore set out to harness these properties inside of an atmospheric water harvester. This new apparatus was designed to take advantage of the initial, fastest part of the adsorption process, followed by desorption of the partially loaded MOF under forced convective heating. To do so, the device was built around a fan-equipped exchanger hosting 0.433 kg of activated MOF-303 powder, packed into 40 4.5 × 4.5 × 0.125 in^3 (10.16 × 10.16 × 0.317 cm^3) beds supported by 10 trays and assembled into a removable cartridge, which was further fitted with heating strips (see the Methods section and Section S5 for details). The cartridge exhibited five channels for convective desorption and six channels for convective adsorption, and each channel had a hydraulic diameter of 0.5 in. (1.27 cm). The circulation of water molecules through this exchanger, which was primarily designed to allow the use of MOF as a powder, is illustrated in Figure 4a. Importantly, the packing porosity of the sorbent bed in the exchanger matched the one of the powder studied by TGA (∼0.7), and the air flow was found to be laminar at all times in both cases (Sections S4.2 and S5.2). The dynamic behavior of the exchanger was first investigated in a series of laboratory experiments. During desorption, ambient air was propelled uniformly across the unit through forced convection at ∼1 CFM (cubic foot per minute), and the MOF bed was concurrently heated to 80−120 °C to trigger the release of water vapor. The generated hot

and humid air could subsequently be transferred to a compressor-based condenser (Figure S56). During the adsorption phase, ambient air was propelled through the MOF exchanger in an orthogonal direction compared to the desorption phase (cross-flow configuration), and the dehydrated MOF extracted vapor from the air by capturing water molecules in its pores. The evolution of temperature and RH during a WHC was monitored by thermocouples and humidity sensors at different locations in the harvester (Figure 4b and Figures S57 and S58). To investigate the sorption kinetics in the MOF bed, variations in the mass of the exchanger associated with water adsorption and desorption were monitored over time at different relative humidities (Figure 4c,d). Active heating of the MOF bed during desorption resulted in a fast process where, independent of ambient conditions, a saturated bed could be desorbed in less than 3 h (Figure 4c). We note that MOF-303 was only partially desorbed under these conditions and released at best 85% of its total uptake, which can be rationalized by the presence of a spatial heat gradient inside the exchanger during the desorption step, especially around the edges of the exchanger Figure 4b and Figure S58), resulting in parts of the MOF not being exposed to sufficiently high temperatures for complete desorption. Furthermore, as expected, the adsorption kinetics, displayed in Figure 4d, varied significantly as a function of ambient RH and were found to be consistent with the general trend reported in Figure 3. However, complete water uptake was only achieved after 300 min at 39% RH and 400 min at 32% RH and was not achieved within 450 min at 22% RH. This slower kinetic behavior compared to the one observed in the aforementioned TGA study can be attributed to a less efficient exposure of the MOF to ambient vapor, complicated by the geometry and materials utilized in the full-size device. However, the speed of adsorption and desorption measured in the exchanger was still suitable for operating multiple WHCs per day with the water harvester. The prototype, equipped with MOF-303, was therefore tested indoors under continuous operation for 24 h.

During the experiment, each desorption phase was terminated when the RH at the outlet of the exchanger reached a constant value (typically within 1 h), while the length of each adsorption phase was adjusted as a function of ambient conditions, based on the data presented in Figure 4 (see Section S6 and Figure S59 for more details), and the amount of liquid water collected after each WHC was measured. Under average conditions of 32% RH and 27 °C (Figure S60), the prototype was capable of extracting a total of 1.3 L kg$_{MOF}^{-1}$ after nine WHCs (Figure S61), corresponding to a significant improvement in productivity over the most recent reports on atmospheric water harvesters operating in arid conditions.[36−38] The efficiency of condensation was estimated to be ∼85%, based on the ratio of collected liquid water over desorbed water vapor (measured *in situ* by a precision scale, Figure 4c). Moreover, the modularity and applicability of the device architecture to different sorbents were demonstrated by replacing the cartridge of MOF-303 by a cartridge of Al-fumarate, and the device was again operated continuously for 24 h, at 32% RH and 23 °C (Figure S63). While Al-fumarate exhibits a similar total water uptake compared to MOF-303 under these conditions (Figure 2), it was only able to deliver 0.55 L kg$_{MOF}^{-1}$ (Figure S64), as anticipated from the difference in dynamic behavior between
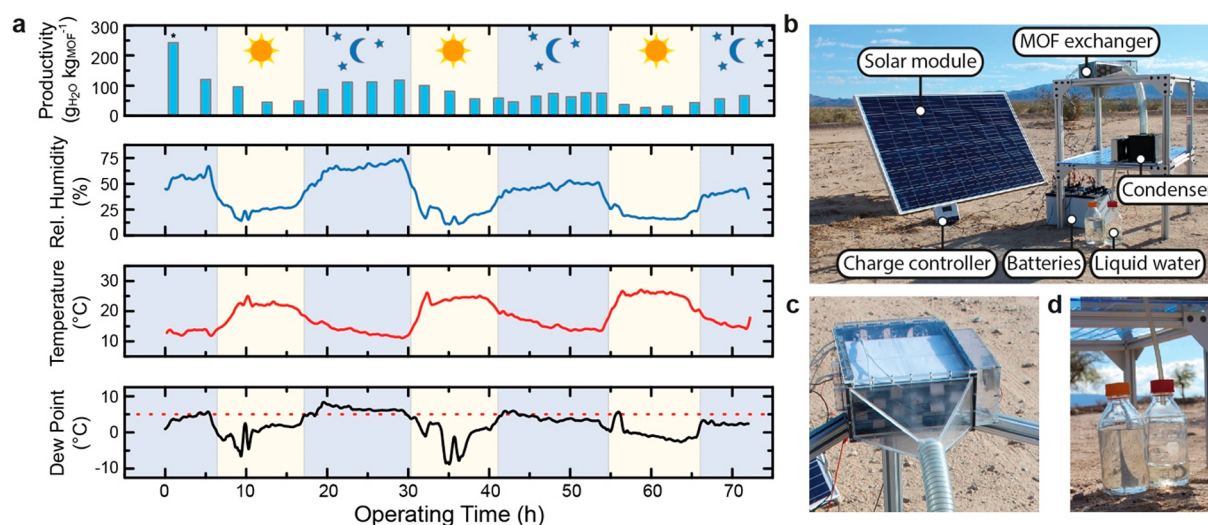
Figure 5. Practical atmospheric water harvesting in the Mojave Desert. (a) Diagram displaying the water harvesting productivity after each water harvesting cycle (WHC), the ambient relative humidity and temperature, and the corresponding dew point. The productivity of the first WHC (*) is higher because the experiment started with a fully saturated MOF bed. All data was measured over the course of three continuous days of operation in the Mojave Desert. The dotted, red line indicates the 5 °C dew point, representing the lower limit for the operating range of direct condensation technologies.[9] (b) Photograph of the water harvester with labeled parts. Close-up views of the MOF exchanger (c) and the water collected under continuous operation (d).

the two materials, emphasizing the crucial importance of fast sorption kinetics to achieve high productivities.

To further demonstrate the viability of the harvester under practical conditions, it was tested in the Mojave Desert, the most arid region in Northern America.[39] The device was operated continuously for 3 days in the hyperarid environment of Twenty-Nine Palms, California (34°10′51.4″ N; 115°54′40.0″ W) between the 17th and 20th of October, 2018, and was powered by four 12 V deep-cycle batteries that could be charged during the day by a photovoltaic module (Figure 5b and Section S8). The productivity after each cycle along with the corresponding ambient conditions are displayed in Figure 5a (see Figure S66 for a more extensive set of sensor data). Importantly, over the 3 days of water collection, the dew point of the ambient air remained below 5 °C (i.e., outside the operating range of direct condensation technologies)[9] for 85% of the time. Remarkably, MOF-303 harvested atmospheric water under conditions as dry as 10% RH and 27 °C, corresponding to a dew point of −4 °C. On average, this stand-alone prototype was able to produce 0.7 L kg$_{MOF}^{-1}$ day^{-1} (Figure 5d), which represents a 10-fold improvement over the previous-generation MOF-assisted water harvester operated in a desert environment.[12]

This work demonstrates that materials for sorbent-assisted water harvesting from desert air should not only be optimized for high uptakes at low relative humidities. Indeed, we show that using MOF-303—a sorbent endowed with low enthalpy of water adsorption (∼52 kJ mol^{-1}) and fast adsorption and desorption kinetics—enables the rapid cycling necessary to perform efficient and high-productivity water collection. These excellent properties were harnessed in a device capable of generating liquid water from arid air, in conditions largely outside of the operational range of direct-cooling condensers, and delivering volumes of water approaching the daily requirements for human consumption. Furthermore, based on the remarkably fast sorption kinetics of free MOF-303 powder (∼10 min per WHC), one can envision the creation of an optimized water harvester capable of producing several tens

of liters per kilogram of MOF-303 per day. These results establish MOFs as a very promising class of materials to make sorbent-assisted atmospheric water harvesting a viable technology to address water scarcity in arid climates.

■ METHODS

Material Synthesis and General Methods. Material synthesis and preparation are described in Section S1. General characterization methods (powder X-ray diffraction analysis, scanning electron microscopy, Ar sorption analysis, and pycnometry) are outlined in Section S2. Water sorption analysis is specified in Section S3.

Water Sorption Dynamics Measurement. The water sorption dynamics measurements were conducted with a TA Instruments SDT Q600 series thermal gravimetric analyzer (TGA). The primary gas inlet was directly connected to a nitrogen tank (Praxair, ultrahigh purity, 99.999%). The secondary gas inlet was used to supply a humidified nitrogen feed by regulating the gas flow using a mass flow controller (Sierra SmartTrak 100) and passing the stream through a gas washing bottle (2 L). The temperature and RH were monitored using high-accuracy thermocouples and humidity sensors downstream of the TGA chamber. The desired humidity was achieved by adjusting the ratio of dry (primary inlet) to humidified (secondary inlet) nitrogen gas flow according to a recorded calibration curve (Figure S28), while maintaining the sum of both flows constant at 250 mL min^{-1}.

For the measurements in thin-layer geometry, ∼1 mg of the MOF sample was loaded in the TGA pan. For the experimental setup in the packed bed geometry, the height of the TGA pan (3 mm) was used as a template to adjust the thickness of the bed by completely filling the pan with the corresponding material. The desired packing porosity was achieved by adjusting the mass of activated sample in the filled TGA pan.

Prior to the adsorption measurement in the TGA, the materials were activated under dry nitrogen flow (250 mL min^{-1}) at 150 °C for the MOFs, 200 °C for SAPO-34, and 300 °C for zeolite 13X until the sample mass was stable for at

least 1 h. After activation, the samples were cooled down to 30 °C under dry nitrogen flow (250 mL min^{-1}). Immediately after 30 °C was reached, the adsorption measurement was started. The temperature during the adsorption was kept constant at 30 °C, and the RH was adjusted by changing the respective ratio of dry to humidified nitrogen flow (Figure S28). Noteworthy, a temperature increase of ∼2 °C was observed during the initial phase of adsorption due to the exothermic nature of this process.

For the desorption measurements, the sorbent was first saturated with water vapor at 40% RH and 30 °C. The desorption measurement was then started immediately after equilibration. The humidified nitrogen gas flow was turned off, the dry nitrogen flow was set to 250 mL min^{-1}, and the temperature was equilibrated at the target temperature (65, 85, 100, or 120 °C). The heating program of the TGA avoided overheating while achieving ∼95% of the target temperature within 4 min.

Water Harvester Assembly and Operation. A removable cartridge containing 10 frames lined with PTFE (pore size 0.45 μm, Sterlitech Corporation), and holding 433 g of fully desorbed sorbent powder (MOF-303 or Al-Fumarate), was wrapped with heating strips (1 in. × 96 in., 120 V, 830 W, BriskHeat B00101080) and installed in a custom-made acrylic enclosure equipped with fans (see Section S5 for more details). The resulting exchanger was connected to a compressor-based condenser (model DV1910E-1C 12 V Pro from Rigid HVAC Co., LTD). The system was powered by four 12 V deep-cycle batteries (140 Ah, PHCC Pro Series). During the desorption step, the exchanger was powered by three of these batteries. Thus, the heating strips were powered by 36 V and drew 5.8 A of current until the temperature at the center of the exchanger was ∼120 °C. They were then switched to a 24 V supply (now drawing 3.9 A) to keep the temperature constant inside of the exchanger. In addition, eight fans located at the rear of the exchanger were initially powered by 12 V (drawing 0.11 A) and switched to 24 V as soon as condensation started to appear on the walls of the exchanger (after ∼10 min, now drawing 0.13 A). The condenser was powered by a different 12 V battery and was drawing 10 A. The desorption was stopped once the RH in the exchanger outlet reached a constant minimum. The liquid water was collected at the bottom of the condenser through an outlet connected to a glass bottle. During the adsorption step, a fan located on the side of the exchanger was powered with a 12 V battery (drawing 0.08 A). The length of the adsorption step was adjusted based on ambient conditions and the kinetics measurements conducted on the exchanger (see Section S7.1). During the operation of the harvester in the Mojave Desert, the exchanger was loaded with 579 g of MOF-303, and the batteries could be charged using a 265 W photovoltaic module (60 cells, 31.0 VDC, 8.56 A, Grape Solar) interfaced with a charge controller (40 A, Model Comet PWM, Grape Solar).

Safety Statement. No unexpected or unusually high safety hazards were encountered.

ASSOCIATED CONTENT

ⓈSupporting Information

The Supporting Information is available free of charge on the ACS Publications website at DOI: 10.1021/acscents-ci.9b00745.

Material preparation and characterization, steady-state and dynamic water sorption analysis, exchanger assembly schematics and characteristics, and additional data and information on the water harvesting device (PDF)

Video showing the water harvesting process (AVI)

AUTHOR INFORMATION

Corresponding Author
*E-mail: yaghi@berkeley.edu.
ORCID ⓞ
Nikita Hanikel: 0000-0002-3292-5070
Eugene A. Kapustin: 0000-0003-4095-9729
Hao Lyu: 0000-0001-7393-2456
T. Grant Glover: 0000-0002-3393-6038
Omar M. Yaghi: 0000-0002-5611-3325

Author Contributions
$^{\nabla}$N.H. and M.S.P. contributed equally.

Notes
The authors declare the following competing financial interest(s): O.M.Y. is a cofounder and E.A.K. is an employee of Water Harvesting Inc.

REFERENCES

(1) World Health Organization. *Health Topics: Health Impact Assessment*; World Health Organization, 2019.

(2) WWAP (UNESCO World Water Assessment Programme). *The United Nations World Water Development Report 2019: Leaving No One Behind*; UNESCO: Paris, 2019.

(3) Hoekstra, A. Y.; Mekonnen, M. M. The Water Footprint of Humanity. *Proc. Natl. Acad. Sci. U. S. A.* **2012**, *109* (9), 3232−3237.

(4) Famiglietti, J. S. The Global Groundwater Crisis. *Nat. Clim. Change* **2014**, *4* (11), 945−948.

(5) Richey, A. S.; Thomas, B. F.; Lo, M.-H.; Reager, J. T.; Famiglietti, J. S.; Voss, K.; Swenson, S.; Rodell, M. Quantifying Renewable Groundwater Stress with GRACE. *Water Resour. Res.* **2015**, *51* (7), 5217−5238.

(6) Mekonnen, M. M.; Hoekstra, A. Y. Four Billion People Facing Severe Water Scarcity. *Sci. Adv.* **2016**, *2* (2), No. e1500323.

(7) Kummu, M.; Guillaume, J. H. A.; de Moel, H.; Eisner, S.; Flörke, M.; Porkka, M.; Siebert, S.; Veldkamp, T. I. E.; Ward, P. J. The World's Road to Water Scarcity: Shortage and Stress in the 20th Century and Pathways towards Sustainability. *Sci. Rep.* **2016**, *6* (1), 38495.

(8) Gido, B.; Friedler, E.; Broday, D. M. Assessment of Atmospheric Moisture Harvesting by Direct Cooling. *Atmos. Res.* **2016**, *182*, 156−162.

(9) Bagheri, F. Performance Investigation of Atmospheric Water Harvesting Systems. *Water Resour. Ind.* **2018**, *20* (Dec), 23−28.

(10) Kim, H.; Yang, S.; Rao, S. R.; Narayanan, S.; Kapustin, E. A.; Furukawa, H.; Umans, A. S.; Yaghi, O. M.; Wang, E. N. Water Harvesting from Air with Metal-Organic Frameworks Powered by Natural Sunlight. *Science* **2017**, *356* (6336), 430−434.

(11) Kim, H.; Rao, S. R.; Kapustin, E. A.; Zhao, L.; Yang, S.; Yaghi, O. M.; Wang, E. N. Adsorption-Based Atmospheric Water Harvesting Device for Arid Climates. *Nat. Commun.* **2018**, *9* (1), 1191.

(12) Fathieh, F.; Kalmutzki, M. J.; Kapustin, E. A.; Waller, P. J.; Yang, J.; Yaghi, O. M. Practical Water Production from Desert Air. *Sci. Adv.* **2018**, *4* (6), No. eaat3198.

(13) Rieth, A. J.; Yang, S.; Wang, E. N.; Dincă, M. Record Atmospheric Fresh Water Capture and Heat Transfer with a Material Operating at the Water Uptake Reversibility Limit. *ACS Cent. Sci.* **2017**, *3* (6), 668−672.

(14) Towsif Abtab, S. M.; Alezi, D.; Bhatt, P. M.; Shkurenko, A.; Belmabkhout, Y.; Aggarwal, H.; Weseliński, Ł. J.; Alsadun, N.; Samin, U.; Hedhili, M. N.; Eddaoudi, M. Reticular Chemistry in Action: A Hydrolytically Stable MOF Capturing Twice Its Weight in Adsorbed Water. *Chem* **2018**, *4* (1), 94−105.

(15) Chen, Z.; Li, P.; Zhang, X.; Li, P.; Wasson, M. C.; Islamoglu, T.; Stoddart, J. F.; Farha, O. K. Reticular Access to Highly Porous Acs-MOFs with Rigid Trigonal Prismatic Linkers for Water Sorption. *J. Am. Chem. Soc.* **2019**, *141* (7), 2900−2905.

(16) Akiyama, G.; Matsuda, R.; Sato, H.; Hori, A.; Takata, M.; Kitagawa, S. Effect of Functional Groups in MIL-101 on Water Sorption Behavior. *Microporous Mesoporous Mater.* **2012**, *157*, 89−93.

(17) Ko, N.; Choi, P. G.; Hong, J.; Yeo, M.; Sung, S.; Cordova, K. E.; Park, H. J.; Yang, J. K.; Kim, J. Tailoring the Water Adsorption Properties of MIL-101 Metal-Organic Frameworks by Partial Functionalization. *J. Mater. Chem. A* **2015**, *3* (5), 2057−2064.

(18) Wright, A. M.; Rieth, A. J.; Yang, S.; Wang, E. N.; Dincă, M. Precise Control of Pore Hydrophilicity Enabled by Post-Synthetic Cation Exchange in Metal-Organic Frameworks. *Chem. Sci.* **2018**, *9* (15), 3856−3859.

(19) Yaghi, O. M.; Kalmutzki, M. J.; Diercks, C. S. *Introduction to Reticular Chemistry: Metal-Organic Frameworks and Covalent Organic Frameworks*; Wiley-VCH: Weinheim, 2019.

(20) Furukawa, H.; Gándara, F.; Zhang, Y.-B.; Jiang, J.; Queen, W. L.; Hudson, M. R.; Yaghi, O. M. Water Adsorption in Porous Metal−Organic Frameworks and Related Materials. *J. Am. Chem. Soc.* **2014**, *136* (11), 4369−4381.

(21) Kalmutzki, M. J.; Diercks, C. S.; Yaghi, O. M. Metal-Organic Frameworks for Water Harvesting from Air. *Adv. Mater.* **2018**, *30* (37), 1704304.

(22) Kalmutzki, M. J.; Hanikel, N.; Yaghi, O. M. Secondary Building Units as the Turning Point in the Development of the Reticular Chemistry of MOFs. *Sci. Adv.* **2018**, *4* (10), No. eaat9180.

(23) Reinsch, H.; Van Der Veen, M. A.; Gil, B.; Marszalek, B.; Verbiest, T.; De Vos, D.; Stock, N. Structures, Sorption Characteristics, and Nonlinear Optical Properties of a New Series of Highly Stable Aluminum MOFs. *Chem. Mater.* **2013**, *25* (1), 17−26.

(24) Cadiau, A.; Lee, J. S.; Damasceno Borges, D.; Fabry, P.; Devic, T.; Wharmby, M. T.; Martineau, C.; Foucher, D.; Taulelle, F.; Jun, C.-H.; Hwang, Y. K.; Stock, N.; De Lange, M. F.; Kapteijn, F.; Gascon, J.; Maurin, G.; Chang, J.-S.; Serre, C. Design of Hydrophilic Metal Organic Framework Water Adsorbents for Heat Reallocation. *Adv. Mater.* **2015**, *27* (32), 4775−4780.

(25) Krajnc, A.; Varlec, J.; Mazaj, M.; Ristić, A.; Logar, N. Z.; Mali, G. Superior Performance of Microporous Aluminophosphate with LTA Topology in Solar-Energy Storage and Heat Reallocation. *Adv. Energy Mater.* **2017**, *7* (11), 1601815-1−1601815-8.

(26) Wang, S.; Lee, J. S.; Wahiduzzaman, M.; Park, J.; Muschi, M.; Martineau-Corcos, C.; Tissot, A.; Cho, K. H.; Marrot, J.; Shepard, W.; Maurin, G.; Chang, J.-S.; Serre, C. A Robust Large-Pore Zirconium Carboxylate Metal-Organic Framework for Energy-Efficient Water-Sorption-Driven Refrigeration. *Nat. Energy* **2018**, *3*, 985−993.

(27) Lenzen, D.; Zhao, J.; Ernst, S.-J.; Wahiduzzaman, M.; Inge, A. K.; Fröhlich, D.; Xu, H.; Bart, H.-J.; Janiak, C.; Henninger, S.; Maurin, G.; Zou, X.; Stock, N. A Metal−Organic Framework for Efficient Water-Based Ultra-Low-Temperature-Driven Cooling. *Nat. Commun.* **2019**, *10* (1), 3025.

(28) Leung, E.; Müller, U.; Trukhan, N.; Mattenheimer, H.; Cox, G.; Blei, S. Process for Preparing Porous Metal-Organic Frameworks Based on Aluminum Fumarate. U.S. 2012/0082864, 2012.

(29) Solovyeva, M. V.; Gordeeva, L. G.; Krieger, T. A.; Aristov, Y. I. MOF-801 as a Promising Material for Adsorption Cooling: Equilibrium and Dynamics of Water Adsorption. *Energy Convers. Manage.* **2018**, *174* (Oct), 356−363.

(30) Hossain, M. I.; Cunningham, J. D.; Becker, T. M.; Grabicka, B. E.; Walton, K. S.; Rabideau, B. D.; Glover, T. G. Impact of MOF Defects on the Binary Adsorption of CO2 and Water in UiO-66. *Chem. Eng. Sci.* **2019**, *203*, 346−357.

(31) Hossain, M. I.; Glover, T. G. Kinetics of Water Adsorption in UiO-66 MOF. *Ind. Eng. Chem. Res.* **2019**, *58* (24), 10550−10558.

(32) Kärger, J.; Wang, Y. Gas Adsorption in Metal-Organic Frameworks. In *Gas Adsorption in Metal-Organic Frameworks*; Glover, T. G., Mu, B., Eds.; CRC: Boca Raton, FL, 2019; pp 109−217.

(33) Kärger, J.; Ruthven, D. M. *Diffusion In Zeolites and Other Microporous Solids*; Wiley: London, UK, 1992.

(34) Kärger, J.; Binder, T.; Chmelik, C.; Hibbe, F.; Krautscheid, H.; Krishna, R.; Weitkamp, J. Microimaging of Transient Guest Profiles to Monitor Mass Transfer in Nanoporous Materials. *Nat. Mater.* **2014**, *13* (4), 333−343.

(35) Titze, T.; Chmelik, C.; Kullmann, J.; Prager, L.; Miersemann, E.; Gläser, R.; Enke, D.; Weitkamp, J.; Kärger, J. Microimaging of Transient Concentration Profiles of Reactant and Product Molecules during Catalytic Conversion in Nanoporous Materials. *Angew. Chem., Int. Ed.* **2015**, *54* (17), 5060−5064.

(36) Ji, J. G.; Wang, R. Z.; Li, L. X. New Composite Adsorbent for Solar-Driven Fresh Water Production from the Atmosphere. *Desalination* **2007**, *212* (1−3), 176−182.

(37) Wang, J. Y.; Liu, J. Y.; Wang, R. Z.; Wang, L. W. Experimental Investigation on Two Solar-Driven Sorption Based Devices to Extract Fresh Water from Atmosphere. *Appl. Therm. Eng.* **2017**, *127*, 1608−1616.

(38) Li, R.; Shi, Y.; Shi, L.; Alsaedi, M.; Wang, P. Harvesting Water from Air: Using Anhydrous Salt with Sunlight. *Environ. Sci. Technol.* **2018**, *52* (9), 5398−5406.

(39) Spinoni, J.; Vogt, J.; Naumann, G.; Carrao, H.; Barbosa, P. Towards Identifying Areas at Climatological Risk of Desertification Using the Köppen-Geiger Classification and FAO Aridity Index. *Int. J. Climatol.* **2015**, *35* (9), 2210−2222.